RSC Advances

This is an *Accepted Manuscript*, which has been through the Royal Society of Chemistry peer review process and has been accepted for publication.

Accepted Manuscripts are published online shortly after acceptance, before technical editing, formatting and proof reading. Using this free service, authors can make their results available to the community, in citable form, before we publish the edited article. This *Accepted Manuscript* will be replaced by the edited, formatted and paginated article as soon as this is available.

You can find more information about *Accepted Manuscripts* in the Information for Authors.

Please note that technical editing may introduce minor changes to the text and/or graphics, which may alter content. The journal's standard Terms & Conditions and the Ethical guidelines still apply. In no event shall the Royal Society of Chemistry be held responsible for any errors or omissions in this *Accepted Manuscript* or any consequences arising from the use of any information it contains.

ROYAL SOCIETY OF CHEMISTRY

www.rsc.org/advances

Regrowth of Ge consisting of different degree of damage under thermal and athermal treatment

***Sonu Hooda*[1], *B Satpati*[2], *Tanuj Kumar*[3], *Sunil Ojha*[1], *D. Kanjilal*[1] and *D. Kabiraj*[1]**

[1]*Inter-University Accelerator Centre, Aruna Asaf Ali Marg, New Delhi-110067, India*

[2] *Saha Institute of Nuclear Physics, 1/AF, Bidhannagar, Kolkata-700064, India*

[3] *Central University of Haryana, Jant-Pali, Mahendergarh, Haryana-123029, India*

Abstract

In this report, the damage recrystallization of pre-damaged Ge sample is extensively investigated under steady state thermal annealing and ultra-fast thermal spike assisted annealing generated by high energy ions. The Ge (100) single crystal samples were pre-damaged using 100 keV Ar ions implantation. Three set of pre-damaged Ge samples with sub-threshold (set A), threshold (set B) and above threshold (set C) doses of amorphization, as estimated by Rutherford Backscattering spectrometry in channeling mode (RBS/C), were suitably selected. Cross-sectional Transmission Electron Microscopy (XTEM) images show distributed damaged pockets within crystalline surrounding in case of as-damaged set A sample and completely damaged layer in set C sample. These samples were used to study regrowth of damage by (i) vacuum annealing at temperatures ranging from 373 K to 873 K for 30 minutes each (ii) 100 MeV Ag ions irradiation assisted annealing at four different temperatures 100 K, 300 K, 373 K and 473 K. After 100 MeV Ag ions irradiation, set A samples have undergone complete recrystallization at 473 K. A similar recrystallization, however less in magnitude, is also observed in set-B sample with increase in temperature. In set C samples, interestingly, nanowire formation was observed instead of recrystallization when irradiated at 100 K and 300 K but recrystallization is observed at high temperature irradiation. Though it is much lower than that of set A and set B samples. The Arrhenius plot of recrystallized fraction revealed the reduction of activation energy of recrystallization by a substantial factor due to thermal spike assisted recrystallization.

Introduction

Germanium is a very significant material used for various useful applications in numerous fields of nanotechnology [1-2] and it is important for high-mobility nanodevice applications [3-4]. The band gap of Ge is suitable for photo-absorption at communication

RSC Advances Accepted Manuscript

wavelength [5-6]. This makes it attractive for the fabrication of high-quality photodetectors [7-8]. Further applications of Ge includes nanoscale transistors[9], high efficiency anodes for lithium ion batteries[10-11] and high performance electronic devices [12]. For device technologies, doping of a semiconductor is required. But the energetic ions in turn induce amorphization or damage creation in the lattice which is required to be annealed or recovered [13]. Low energy ion interactions are dominated by elastic processes or nuclear stopping, resulting in the ballistic atomic displacements of substrate atoms[14]. Hence damage creation is attributed to energy transfer to the atomic structure, which results in displacement of target atoms from their lattice sites. Ion implantation and recovery process has been studied extensively by various groups during past decade [15-17]. Ion beam induced recrystallization was also studied in Si [18] and the possible role of electronic energy loss on recrystallization in Si was reported. On the other hand, besides of numerous application there are few relevant reports on study of damage formation in Ge due to low and high energy ion implantation e.g. 56 keV B ions [19], 185 MeV Au ions [20] and 20 keV B ions [21]. The main difference between Ge and Si is that Ge is identified to become porous after a critical dose [22-23]. There is a lack of extensive study on ion implantation induced defect formation and their thermal annealing in Ge. Decoster *et al.* [24] investigated the damage evolution due to implantation and its recovery via thermal annealing. Crystallization from a disordered structure is eventually a diffusive process and it is strongly temperature dependent. Hence, thermal annealing is the traditional method for elimination of implantation-induced defects and for activation of implanted impurity. However, in the case of Ge-based devices the high temperature annealing is not advisable [25]. Now a days, solid phase epitaxial growth[26], electron, flash lamp[27], laser [28] and swift heavy ions (SHI) [29-30] irradiation are most widely used methods for recrystallization of a-Ge due to their uniformity in depth distribution. The evolution of pre-damaged Ge and recrystallization behavior due to the effect of energetic ions, at room temperature, has been reviewed earlier by our group [29]. Such interactions are governed by inelastic processes where electronic stopping is dominating which results in the excitation and ionization of Ge atoms. In case of irradiation with SHI, the major part of energy is deposited to the loosely bound electronic subsystem and then transferred to the atomic subsystem through electron–phonon coupling [31]. The elastic processes with dominating nuclear stopping, are negligible in this regime. So, the annealing of pre-existing damage is expected.

In this work, we prepared three set of Ge samples in which we deliberately introduced defined degree of damage such that first set (A) with damage of ~0.25 displacements per atom (dpa) contains isolated amorphous pockets surrounded by crystalline material, second

RSC Advances Accepted Manuscript

set (B) with damage of ~0. 5 dpa contains inter-connected amorphous zones and third set (C) with damage of ~7 dpa contains fully amorphous layer. Displacements per atom are estimated on the basis of theoretical formulation followed in TRIM simulation [32]. The recrystallization dynamics of these pre-damaged Ge samples is reported here under ultra-fast thermal spike assisted annealing produced by 100 MeV Ag ions irradiation at variable temperature and compared with steady state thermal annealing at temperature up to 873 K. The recrystallization is characterized by RBS/C, miro-Raman spectroscopy and supported by X-TEM.

Experimental

In order to understand and quantify the damage recovery and ionization effects on it in better way, different pre-damaged states were introduced in Ge by means of low-energy ion irradiation with 100 keV Ar^+. The high nuclear stopping power S_n (0.6 keV nm^{-1}) [32] is responsible for the displacement damage production. Different fractional damage levels were introduced using different doses, with peak disorder at a depth of ~80±10 nm. Three set of samples with damage of 0.25 dpa, 0.5 dpa and 7 dpa at the damage peak were chosen. These samples with specific degree of damage, corresponds to Ar ion fluences of 4×10^{13} (set A), 8×10^{13} (set B) and 1×10^{15} (set C) ions cm^{-2} respectively. RBS/C results demonstrate the sample irradiated at 8×10^{13} ions cm^{-2} (set B) just touches the random spectrum. This indicates irradiation at threshold fluence of amorphization. The evolution of the crystalline damage resulting from the Ar ion irradiation was studied as a function of ion dose by Rutherford Backscattering Spectrometry in channeling mode (RBS/C). The RBS/C experiments were carried out at Inter University Accelerator Centre (IUAC), Delhi using 2 MeV He ions. RBS/C results demonstrate that channeled yield of the sample irradiated at 8×10^{13} ions cm^{-2} (set B) just touches the random spectrum. This indicates irradiation at threshold dose of amorphization. The depth distribution of defects from RBS/C spectra was computed using simulation code named DICADA [33], which is based on the discontinuous model of dechannelling. The transmission electron microscopy (TEM), using FEI TF30, S-TWIN microscope operating at 300 kV equipped with a GATAN Orius CCD camera, was used to investigate the state of damage in these samples.

The damage recovery in these pre-disordered states was studied by sequential ionization assistance at variable temperature and over a range of ion doses. Hence, the three set of samples were irradiated with 100 MeV Ag ions from 15 UD Pelletron Accelerator at

RSC Advances Accepted Manuscript

IUAC Delhi, at temperatures ranging from 100 K to 473 K. Such experimental conditions provide a controlled investigation to evaluate the ionization effects separately without introducing considerable displacement damage due to elastic collisions. Moreover, these selected sets of damaged samples were annealed in vacuum with a base pressure of 1×10^{-6} mbar for 30 minutes at temperatures ranging from 373 K to 873 K to study recrystallization under steady state thermal annealing. The rate of increase of temperature was kept 5 ºC min^{-1}. As nanowires formation was observed after irradiation of set C samples at room temperature[29]. The effect of post Ag ions irradiation annealing is also studied in these samples and hence annealed up to 873 K in vacuum environment.

The evolution of the crystallized fraction resulting from thermal annealing and athermal annealing was studied as a function of irradiation dose and irradiation temperature using RBS/C. For detailed quantitative analysis of change in damage fraction, simulation of the RBS/C spectra was performed using DICADA[33]. Micro Raman spectroscopy of the samples is carried out using Renishaw inVia Raman spectrometer for 514.9 nm wavelength laser with spot size of 1-2 µm.

Results

The ion beam induced amorphization and then subsequent damage recovery under thermal as well as athermal (ion beam assisted) annealing processes in Ge (100) were analyzed with the help of RBS/C, Raman and high-resolution TEM analysis. Cross-sectional TEM (XTEM) image recorded for as-damaged set 'A' sample, which were prepared using 100 keV Ar for the fluence of 4×10^{13} ions cm^{-2}, show the isolated distributed damaged pockets surrounded by crystalline material (see figure 1(a)) up to a thickness of ~110±10 nm from the surface side as shown in inset I in figure 1(a). The average size of damage pockets was estimated and found to be of size 4-5 nm. Some of them are pointed out in this image. These damaged regions are surrounded by nanocrystalline particles with size much higher than the damaged pockets. The inset II in figure 1(a) is the Fast Fourier Transform (FFT) pattern of as-damaged set A sample collected from the region highlighted with red color rectangle in the image. It is showing diffused rings along with presence of some crystal spots. Figure 1(b) is the TEM image of as damaged set C sample prepared for fluence 1×10^{15} ions cm^{-2} of 100 keV Ar, showing uniform amorphous layer of thickness ~170±10 nm consisting of nano-crystallites. Hence, different disorder profiles of ~0.25, 0.5 and 7 DPA were produced using 100 keV Ar ions in corresponding set of samples such that the samples

RSC Advances Accepted Manuscript

consist of isolated damaged regions, joining damaged regions and completely amorphous layer respectively.

Figure 2 shows the cross sectional HR-TEM image of set B sample annealed at 873 K. One can see clearly from this lattice image that substantial defect annihilation has happened after thermal treatment. The HRTEM image is collected from the near surface region and it is showing uniform morphology with very few defects and single crystalline in nature. However, there are few residual defects like dislocation loops in the pre-damaged layer are present after annealing as shown in the low magnification XTEM image in inset I of figure 2. FFT pattern (shown in the inset II) taken from the highlighted region with rectangle in this HRTEM image showing distinct spot pattern which again confirm the crystalline quality of layer. The residual defects are lying at a depth of ~40 nm from the surface side. Moreover, the material is recrystallized above and below the layer containing these defects. From the contrast of the low magnification TEM image in inset I, the presence of an implanted layer is clear.

Micro-Raman and RBS/C spectra were recorded for set A, B and C samples in as-damaged state as well as after thermal and athermal annealing to complete the study over the whole range of samples. Figures 3(a) and 3(b) show the micro-Raman spectra of set B and set C samples respectively, after thermal treatment. The spectrum of c-Ge wafer is also shown for comparison. The peak at 301 cm^{-1} in pristine Ge is related to the longitudinal optical (LO) phonon mode of c-Ge. In the as-damaged samples a broad band centered around at ~270 cm^{-1} is observed, which corresponds to the LO phonon mode of amorphous Ge phase. For set B and C samples, clear indication of recrystallization is observed from Raman spectra after annealing. The increasing intensity of c-Ge peak (301 cm^{-1}) with temperature, indicates an increasing contribution of crystalline phase at the cost of amorphous phase. In set B samples, recrystallization starts after annealing at 573 K as the peak corresponding to c-Ge starts to appear (see Fig. 3(a)). Further increase in temperature results in increase in intensity and sharpness of peak at 301 cm^{-1} which corresponds to the un-damaged (c-Ge) sample. Figure 3(b) shows the appearance of c-Ge peak at 301 cm^{-1} at 773 K that became strong and sharper at 873 K which emphasizes the damage recovery in set C samples with increasing annealing temperature. However, amorphous component gives rise to a tail in this peak. The penetration depth of laser used for Raman measurements was found to be ~20 nm in Ge. This clearly indicates the near surface recrystallization after annealing. This is also reflecting from the HRTEM image of this sample shown in figure 2. The re-crystallization results were further

RSC Advances Accepted Manuscript

corroborated by RBS/C. Thermal agitation induced recovery is manifested as a reduction in disorder with increasing temperature. The damage recovery behaviour in the pre-damaged samples with D_0=0.5 dpa (set B) and 7 dpa (set C), evaluated with the help of simulation code DICADA, are shown in figure 4. Up to 473 K, no significant effect on damage profile was observed. In set B samples, though the width of damage profile starts reducing after annealing at 573 K, reduction in amplitude of the damaged regions is observed only on 773 K as shown in figure 4(a). This emphasizes that the simple defects in tail regions start annealing at lower temperature. However, the complex defects start annealing only at 773 K. The width of damage profile is reduced from 190 nm to 50 nm but the peak damage is reduced by 90%. Moreover, the damage peak maxima at ~40 nm from surface side in figure 4(a) indicates some remnant defects in the set B sample, even after annealing at 873 K, which enhanced the backscattered yield of RBS/C spectrum. This result is supported by the TEM result shown in figure 2 where defects as the end product of annealing treatment at 873 K are present at depth of ~40 nm below surface. Figure 4(b) shows the reduction of damage profile width at 773 K but onset of annealing of peak damage at 873 K for set C samples. The width of damage profile reduced from ~210 nm to ~53 nm at 873 K. Since the material is not completely recrystallized yet; consequently the asymmetry is present in the LO peak related to c-Ge (301 cm^{-1}) in the Raman spectrum of set C sample annealed at 873 K as shown in figure 3 (b).

In case of 100 MeV Ag ions irradiation assisted annealing; RBS/C and Raman spectroscopy results indicate significant recrystallization even at room temperature. The recovery process was prominent in set A samples but in set B samples recovery was observed across amorphous-crystalline boundary but not in the central zone of the damage region. However, in set C samples no recrystallization took place after Ag ions irradiation up to highest dose of 1×10^{14} ions cm^{-2}. Instead, the region turned into nanowires after 100 MeV Ag ions irradiation as we have reported earlier [29]. As a consequence of sequential high temperature Ag ion irradiations for various ion doses, significant damage annealing is observed in the pre-damaged region with the help of detailed analysis of RBS/C and Raman spectra. Figure 4 shows the micro-Raman spectra of the corresponding set A samples irradiated at three different substrate temperatures along with the undamaged Ge sample. In as-damaged sample, a broad band is observed at around 270 cm^{-1} which is related to the LO phonon mode of a-Ge phase along with a small peak at 301 cm^{-1} demonstrating co-existence of both crystalline and amorphous phases. The peak related to crystalline component increases with increasing Ag ion dose indicates increasing recrystallization with irradiation.

RSC Advances Accepted Manuscript

We also observe that recrystallization is more efficient when samples are irradiated at higher temperature. From Raman spectroscopy results shown in figure 5(a), it can be concluded that in set A samples, the recrystallization of defects starts even at 100 K. Considerable damage recovery is observed after Ag ions irradiation at room temperature. On further increasing substrate temperature to 373 K results in increasing intensity and sharpness of peak at 301 cm^{-1}; though amorphous component produces only a tail in this peak revealing near complete recrystallization as shown in figure 5(b). Figure 6 (a, b) show the damage profile, of set A samples irradiated at temperatures of 373 K and 473 K respectively, extracted from RBS/C data using DICADA. The data corresponding to the undamaged Ge sample is also shown for comparison. The profile in figure 6(a) shows the reduction in disorder by more than 50% at the damage peak maxima at highest fluence used when irradiated 373 K. This recovery is more than 95% in case of irradiation at 473 K as shown in figure 6(b). Hence these results corroborate the Raman observations. Complete recrystallization is marked in set A samples at ion dose of 1×10^{14} ions cm^{-2} at 473 K with the help of Raman spectroscopy (figure 5(c)) and RBS/C results (figure 6(b)).

Figure 7(a) and 7(b) shows the Raman spectra of set C samples after irradiation with Ag ions at 373 K and 473 K as no recovery of defects was observed up to room temperature irradiation [29]. In the as-damaged sample, the presence of the broad band corresponding to a-Ge is observed at around 270 cm^{-1} and non-existence of peak at 301 cm^{-1} related to crystalline phase, emphasized the complete amorphization of Ar ion irradiated near surface layer of Ge. On irradiating with Ag ions at 373 K, the LO mode corresponding to c-Ge starts to appear at ~301 cm^{-1} along with the a-Ge peak. The intensity of c-Ge peak increases with increase in irradiation dose as shown in figure 7(a). It reveals the onset of recrystallization and co-existence of amorphous and crystalline phases. Figure 7(b) reveals that increasing irradiation temperature to 473 K results in increase in crystal fraction which further increases with ion dose. At highest dose 1×10^{14} ions cm^{-2}, c-Ge LO peak becomes sharper with reduction of tail in lower wave number shift side showing further recrystallization of the damaged region. However, an asymmetry is still present in the LO peak related to c-Ge which signifies the presence of defects in the irradiated region as evident from RBC/C result.

Similar analysis of set B samples was performed using RBS/C and Raman spectroscopy results as shown in figure 8. The simulated disorder concentration for all set B samples using software DICADA is plotted as a function of ion dose is shown in figure 8(a, b and c) for different temperatures. Figure 8(a) shows that in these samples, damage recovery is observed

RSC Advances Accepted Manuscript

in the tail region only; however there is no damage reduction at the peak maximum when irradiated at 100 K. Here, the FWHM of the damaged region is reduced from 190.4 nm to 158.6 nm after irradiation at 1×10^{14} ions cm^{-2}. This reveals that the damaged region present in set B samples reduced. The reduction took place from both surface and bulk side highlighting the recrystallization in pre-damaged samples after SHI irradiation. It is found that recrystallization is less effective at peak damaged region. This damage recovery increases with ion dose as corroborated by Raman spectra shown in figure 8(d) which show the appearance and strengthening of c-Ge peak with fluence. With further increase in irradiation temperature to 373 K and 473 K, recrystallization of defects increases as shown in figure 8 (b-c and e-f). The width of damaged profile is reduced from 190.4 nm to 136.6 nm and area under damaged region is reduced by ~50% after irradiation at 473 K for ion fluence of 1×10^{14} ions cm^{-2}. At these temperatures, the LO peak for c-Ge becomes sharper with reduction of asymmetry in tail showing further recrystallization of the damaged region. Moreover, in set B we have observed shrinking of amorphous regions from the boundaries and in the central zone as well. However, no recrystallization was observed in vacuum annealed set B and set C samples up to 473 K as shown in figure 3 and 4. It reveals that ion induced thermal spike assist the recrystallization of damaged layer at much lower temperature. Though, the recrystallization is not complete and this region still constitutes defects as demonstrated by the damage profile and asymmetry in Raman peak (at 301 cm^{-1}) at 473 K even at highest dose of 1×10^{14} ions cm^{-2}. The recrystallization is relatively rapid in terms of the Ag ions fluence and irradiation temperature for the less damaged crystals i.e. those with dpa ~0.25 and relatively slow for the heavily damaged region i.e. those with disorder of dpa~0.5 and 7 which corresponds to threshold and above threshold fluences of amorphization in this study.

The recovery from disorder as a function of temperature was calculated for thermally annealed samples. The recrystallization rate has been measured at damage peak maximum and plotted for set B and set C samples. Here, the rate of recrystallization is found to increase exponentially with lower rate in set C samples as compared to set B. Similarly, the recrystallization rate was calculated from the change in the amount of disorder as a function of ion dose for Ag ion irradiated samples. From these calculations, one can calculate the epitaxial recrystallization rate between two successive ion doses ϕ_i and ϕ_{i+1} for pre-damaged samples at the peak damage z. The recrystallization rate has been expressed as [34]

$$N(z,\phi) = \frac{D(z,\phi_i) - D(z,\phi_{i+1})}{\phi_{i+1} - \phi_i} \qquad \text{............ (1)}$$

RSC Advances Accepted Manuscript

Where $D(z,\phi_i)$ is the amount of disorder at depth z and dose ϕ_i. Using the above formulism the recrystallization rate was found to be increased rapidly in set A samples and the growth rate is slower with increase in amount of initial damage. The activation energy was also calculated from the Arhenius plot of recrystalled fraction with inverse of temperature for thermally annealed set B and C samples, shown in Fig. 9(a) and 9(b) respectively and for Ag irradiated case in figure 8(c). In case of thermally annealed samples, the activation energy was found to be ~0.165 eV and ~0.23 eV for set B and set C samples respectively. On the other hand, the activation energy calculated in irradiated samples was found to be reduced to ~0.06 eV and ~0.05 eV for set B and C samples, respectively. However, the activation energy in set A samples after irradiation was found to be ~0.07 eV. Here Raman results show substantial damage recovery as compared to RBS/C. This may be due to the higher sensitivity of RBS/C as compared to Raman spectroscopy for short range disorder introduced by presence of high density of stacking faults and dislocations in the re-crystallized Ge region.

Besides recovery of a-Ge after Ag ion irradiation, there is remnant stress in the recrystallized Ge material. This is signified by shift in the Raman peak related to c-Ge towards the lower wave numbers compared to single crystal Ge which is stress free. It consequently reveals the appearance of tensile stress in the Ge lattice due to the micro-structural changes during the recrystallization process. The shifts and corresponding stress values are average values resulting from the laser scattering which occur over the damage distributed throughout volume. The magnitude of this tensile stress (σ) is estimated by using the following equation from in plane stress model [35]: $\sigma(\text{MPa}) = -250\Delta\omega$ (cm^{-1}), where $\Delta\omega=\omega_I-\omega_o$. In this expression, ω_o and ω_I are the Raman shift related to the c-Ge peak of the stress-free single crystal and recrystallized Ge samples, respectively. For all three set of samples, the stress was quantified using the above equation and its variation with irradiation temperature is shown in Fig. 9(d). From figure 9(d), it can be concluded that the stress is reduced with increase in temperature though the rate of reduction is higher for samples having higher initial damage (set C). Furthermore, the stress is not removed completely in set B and set C samples even after irradiation at 473 K. It is due to the presence of significant isolated damaged zones. In set A samples, the remnant stress is very less which corroborates the RBS/C results showing approximately complete recrystallization.

The XTEM image as shown in figure 10(a) reveals that after Ag ions irradiation at room temperature to ion dose of 1×10^{14} Ag ions cm^{-2}, the pre-damaged layer in set C sample transformed to nanostructures like void and nanowires. The Ag ions results in melting of a-

RSC Advances Accepted Manuscript

Ge due to thermal spike generation. Consequently void formation took place in a-Ge material, during resolidification from melt phase, due to high density of Ge in molten phase[36]. These voids add upto surface and remnant material results in nanowires structures. This phenomenon is explained in more detail in the earlier report[29]. The inset in figure 10(a) is the SAED pattern of nanowire showing the amorphous nature of these nanowires. The results presented above clearly establish that in case of samples damaged at 7 DPA, high temperature irradiation induce recrystallization but irradiation at temperatures up to room temperature induce nanowire and void formation. To study the effect of post irradiation annealing in these samples consisting of nanowires, the micro-Raman investigations were carried out after thermal annealing. Figure 10(b) shows the Raman spectra of annealed samples along with c-Ge. These spectra reveal that initially the nanowires were amorphous in nature and they sustain with their amorphous phase after annealing up to a temperature of 673 K as the Raman spectra was showing only LO phonon peak related to a-Ge at ~270±2 cm^{-1}. However, the c-Ge peak emerges at annealing temperature of 773 K which becomes sharper and stronger at 873 K as shown in inset of figure 10(b). Hence, Raman measurement emphasized that thermal annealing exhibits partial recrystallization of nanowires because of presence of asymmetry in LO peak corresponding to c-Ge even at 873 K. The pores and voids in Ge are highly stable upon annealing therefore recrystallization of nanowires does not account for the alteration of the void structures. This observation also accounts for the onset of recrystallization of a-Ge material at 773 K no matter if it is in bulk form or in nanowire form. In set C sample the two distinct observations are made in the samples irradiated at elevated temperature as compared to irradiation at room temperature: (i) absence of voids and (ii) emergence of crystalline phase.

Discussion

We have observed that irradiation of c-Ge by 100 MeV Ag produce negligible damage which scales with nuclear energy loss (~0.1 keV nm^{-1}). Whereas very high Se (~160*Sn) is insensitive to damage formation even at high irradiation ion fluences of up to 10^{14} cm^{-2}. However, the irradiation of damaged Ge with same ion leads to remarkable structural modifications. We are presenting the results which show that these modifications are also very sensitive to the sample temperature at which 100 MeV Ag ions irradiation is performed. During electronic energy loss, interaction of incident ion with free and bound electrons in a solid leads to formation of energetic secondary electrons. These electrons are confined within a narrow cylindrical target zone around ion path called as ion track. The confinement of these

RSC Advances Accepted Manuscript

electrons depends on electron diffusion length thus modify electron-phonon coupling (g). The coupling term 'g' governs the efficiency with which energy deposited in electronic subsystem is subsequently transferred to lattice sub-system per unit volume and time to increase lattice temperature. The two temperature model can be used to describe the rise in temperature of lattice. The description of two temperature model is based on a set of two coupled heat diffusion equations. One of the equations is for the electronic system and another is for the phonon system which allow one to estimate the peak temperature along ion track in cylindrical geometry [37].

$$C_e(T_e)\frac{\partial T_e}{\partial t} = \frac{1}{r}\frac{\partial}{\partial r}\left[rK_e(T_e)\frac{\partial T_e}{\partial r}\right] - g(T_e - T_a) + A(r,t) \quad ....(2)$$

$$C_a(T_a)\frac{\partial T_a}{\partial t} = \frac{1}{r}\frac{\partial}{\partial r}\left[rK_a(T_a)\frac{\partial T_a}{\partial r}\right] + g(T_e - T_a) + B(r,t) \quad ....(3)$$

Here, r is the radial distance from the path of ion or track radius. $T_{e,\ a}$, $C_{e,\ a}$, and $K_{e,\ a}$ are temperature, specific heat and thermal conductivity for the electronic and atomic subsystems, respectively. All these parametrs and their detailed description is given in our previous report [29]. Numerical solution of these coupled differential equations give time evolution of temperature along the ion track which is plotted in figure 11, at zero distance from ion path and at two irradiation temperature of 300 K and 473 K. The peak track temperature depends on electron-phonon coupling strength i.e. 'g' which is estimated to be 1.2×10^{12} W K^{-1} cm^{-3} and 1×10^{11}W K^{-1} cm^{-3} for amorphous Ge and c-Ge respectively[29]. Consequently, it leads the ion track temperature to reach above melting point in a-Ge whereas it is less than the melting temperature in c-Ge. It may describe the insensitivity of 100 MeV Ag ions irradiation in c-Ge towards damage formation and extensive damage formation in a-Ge as shown in figure 10(a) for set C samples irradiated at 300K.

The results show the molten track formation due to thermal spike generation in a-Ge in both cases. This is understandable from the time evolution of temperature in a-Ge, extracted from thermal spike calculations, as shown in figure 11. This figure clearly shows that the material remains in liquid phase for a time of 2 Pico seconds in both the cases of 300 K and 473 K irradiation. The liquid Ge has a diffusivity of order of 10^{-8} m^2 s^{-1} as reported using simulation studies[38]. During resolidification from melt phase i.e. in region 2 in figure 11, void formation took place in a-Ge during room temperature irradiation, due to high density of Ge in molten phase [36]. However, resolidification in this region II results in recrystallization of the

RSC Advances Accepted Manuscript

amorphous material instead of void formation when the substrate temperature was higher i.e. 473 K. This may be attributed to the quenching rate which is given by $\Delta T/\Delta t$, where ΔT is temperature difference and t is corresponding time. So when the substrate itself is at, say, 473 K then quenching will be slower due to less temperature difference between the spike and substrate such that $(\Delta T/\Delta t)_{473K} < (\Delta T/\Delta t)_{300K}$. Consequently the vacancies may get more time to diffuse which inhibit their agglomeration to form void structures. This scenario can be understood with the help of inset in figure 11 which is the expanded view of region II in figure 10. It indicates the slower resolidification rate for 473 K as compared to 300 K consequently recrystallization due to diffusion of vacancies before their combination to form void.

In partially damaged Ge, where pockets of amorphous Ge is surrounded by c-Ge, when irradiated by 100 MeV Ag ions leads to recrystallization at room temperature for set A sample and for set B sample at higher irradiation temperature. This may be due to synergic effect of both nuclear energy loss and electronic energy loss process where S_n efficiently produces interstitial vacancy pairs at the crystal-amorphous (c-a) interface. Therefore, only those defects generated directly at the c-a interface or nearby it are available for the recrystallization process. So the Ag ion induced additional vacancies reached the interface and could help in enhancing the regrowth process. The number of excess vacancies created by Ag ions is ~10^{18} cm^{-3} as calculated using SRIM[32]. While the vacancies/defects are produced all along the ion track, all of them cannot reach the interface and participate in the recrystallization process. Werner et al. [39] investigated the effect of various parameters on self diffusion in Ge and determined that, under equilibrium conditions, vacancies mediate self-diffusion in Ge. Under thermal equilibrium, the existence of interstitials had not been evidenced. The reason behind this might be related to the higher energy of formation of interstitials as compared to vacancies [40]. However, interstitials participate extensively in self-diffusion under non-equilibrium condition[41].

Conclusion

Three set of samples consisting of different degree of damage introduced by sub-threshold (set A), threshold (set B) and above threshold (set C) doses of amorphization using 100 keV Ar ions were used here. RBS/C, Raman and XTEM analysis of set A, B and C samples after thermal and athermal treatment showed that enhanced recrystallization of damaged region take place after irradiation with 100 MeV Ag ions. However, the rate of

RSC Advances Accepted Manuscript

relative recovery depends on initial disorder level, annealing temperature and ion dose. Hence a relatively strong annealing effect is observed for the less-damaged set A samples. Considerable damage recovery is observed after Ag ions irradiation even at 100 K. While at an irradiation temperature of 473 K, the Ar ion-induced damage is almost fully healed; and the ordered atomic structure is confirmed. For the high-disorder samples set B with 0.5 dpa, a higher irradiation temperature is needed to completely repair the pre-existing damage. Substantial recovery is observed under the Ag irradiations when the temperature increases from 100 K to 473 K, with the disorder levels dropping to ~ 0.75. Additional Ag irradiation is required to fully heal the damaged crystalline structure. Remarkably different results are observed in set C samples, having completely amorphous layer on c-Ge substrate, as 100 MeV Ag ions irradiation form nanowries in a-Ge when irradiated at 100 K and 300 K but there is recrystallization when irradiated at ~500K and above.

Acknowledgement

Ms. Sonu Hooda is thankful to Council of Scientific and Industrial Research (CSIR), India for financial support through fellowship. We would like to thank Dr. Fouran Singh and Mr. Subodh Gautam for help during Raman spectroscopy measurements. Help received from Dr. Parvin Kumar and Mr. Kedarmal during the ion irradiation experiment is gratefully acknowledged.

RSC Advances Accepted Manuscript

Figure Caption

Figure 1. XTEM images of damage creation in 100 keV Ar ions irradiated (a) Set-A sample consisting of isolated damage pockets, the inset I shows the image of whole affected layer, inset II shows the FFT pattern of as-damaged Ge taken from the region marked with rectangle in red color and (b) set C sample.

Figure 2. XTEM image of set B sample after steady state thermal annealing under vacuum condition, at temperature 873 K, it is showing recrystallization in the near surface region. The inset I is the low magnification image of this sample which shows the residual defects at a depth ~33 nm after annealing even at such high temperature. The inset II is the FFT pattern collected from the region highlighted with red rectangle.

Figure 3. Micro-Raman spectra of thermally annealed (a) set B and (b) set C samples showing regrowth of damage after a particular temperature. For comparison, the spectra for 100 keV Ar ion irradiated samples (as-damaged) are also shown in both cases.

Figure 4. Damage profile (extracted from DICADA), as function of annealing temperature, of the steady state thermally annealed (a) set B and (b) set C samples. For comparison, the spectra for 100 keV Ar ion irradiated samples (as-damaged) are also shown in both cases.

Figure 5. Micro-Raman spectra obtained from as amorphized and 100 MeV Ag irradiated set A samples in the temperature range of 100 K to 473 K. The spectrum of pristine (un-implanted) Ge is also shown for reference. The units of the indicated fluences are in ions cm^{-2}.

Figure 6. The damage profile of the ion assisted recrystallized set A samples (extracted from DICADA) as a function of irradiation fluence, for the temperatures of (a) 373 K and (b) 473K, respectively.

Figure 7. Micro-Raman spectra obtained from as amorphized and 100 MeV Ag irradiated set C samples for 373 K and 473 K temperature plotted against ion fluence. The spectrum of pristine (un-implanted) Ge is also shown for reference. The units of the indicated fluences are in ions cm^{-2}.

Figure 8. The damage profile and Micro-Raman spectra as a function of irradiation dose of the ion assisted regrown set B samples for the temperature of 100 K in (a) & (d), 373 K (b) & (e) and for 473K in (c) and (f), respectively.

RSC Advances Accepted Manuscript

Figure 9. Arrhenius plot of regrowth rates for (a) thermally annealed set B (b) thermally annealed set C and (c) 100 MeV Ag induced crystallization, as a function of inverse of temperature (d) Variation of Stress as a function of irradiation temperature, here the lines join the points to guide eyes.

Figure 10. (a) The high resolution TEM image of as-prepared nanowires in a-Ge on c-Ge substrate, inset shows the SAED pattern of nanowire sample (b) Micro-Raman spectra of annealed nanowires plotted for the range of temperature from 373 K to 873 K. Inset shows the expanded Raman spectra showing recrystallization on annealing the nanowires.

Figure 11. The thermal spike calculations of 100 MeV Ag ions in a-Ge, the time evolution of temperature is presented at centre of the track (i.e. at r=0). Inset shows the expanded view of region II.

RSC Advances Accepted Manuscript

Fig. 1

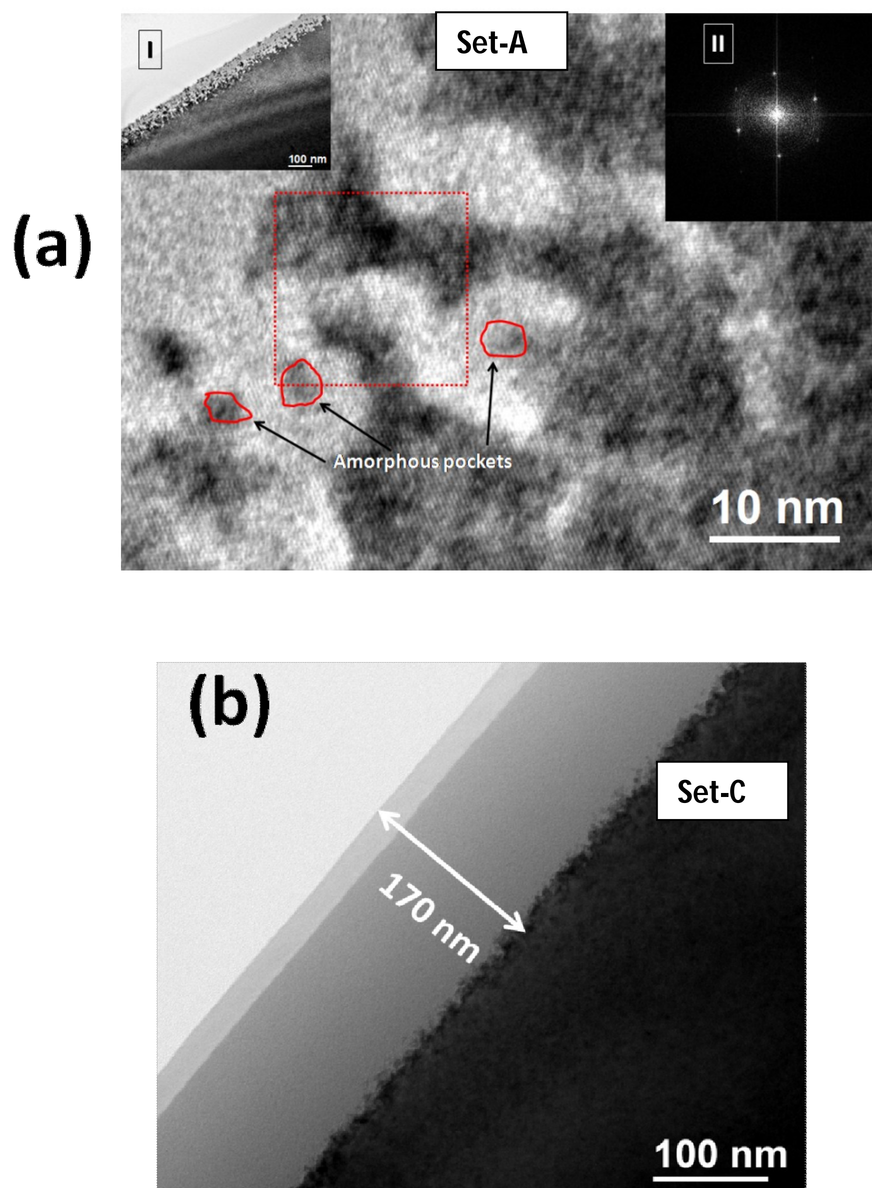

RSC Advances Accepted Manuscript

Fig. 2

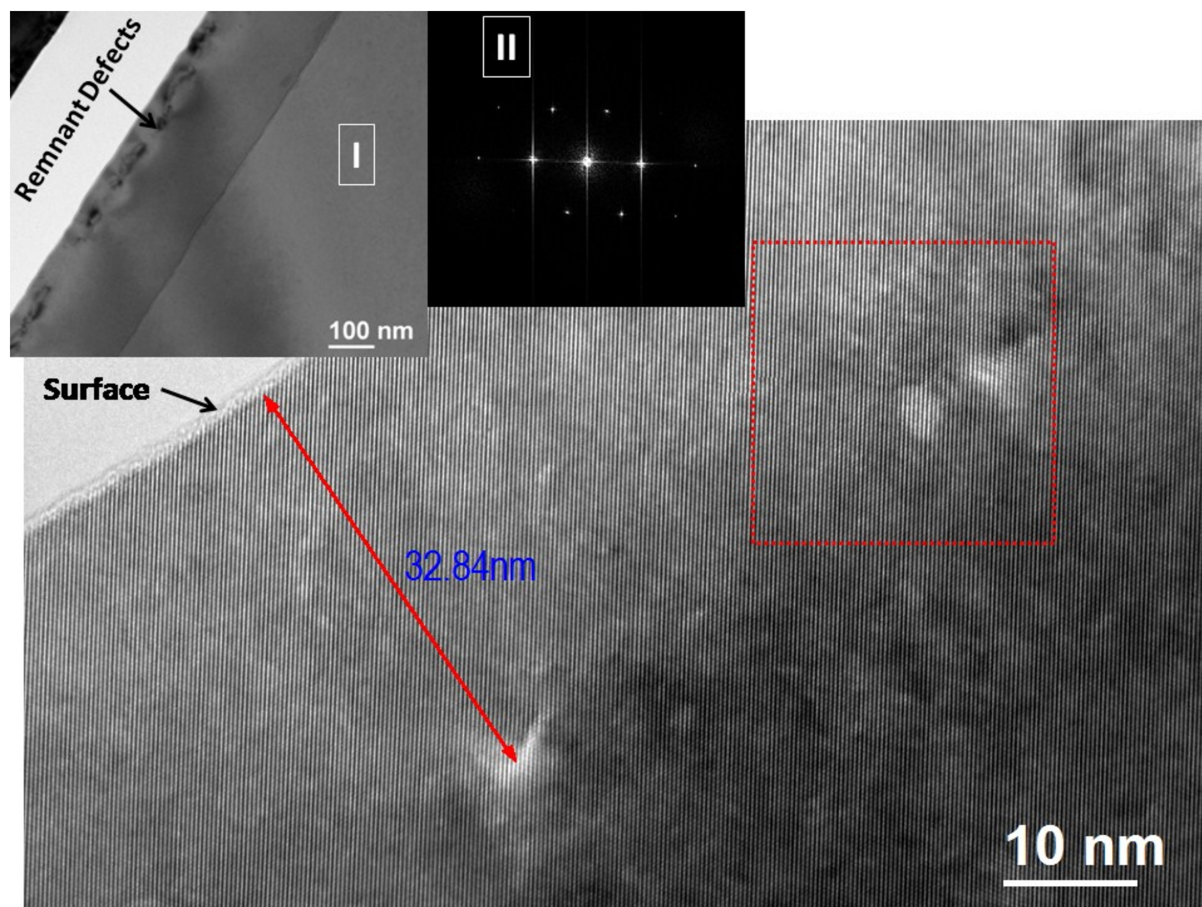

RSC Advances Accepted Manuscript

Fig. 3

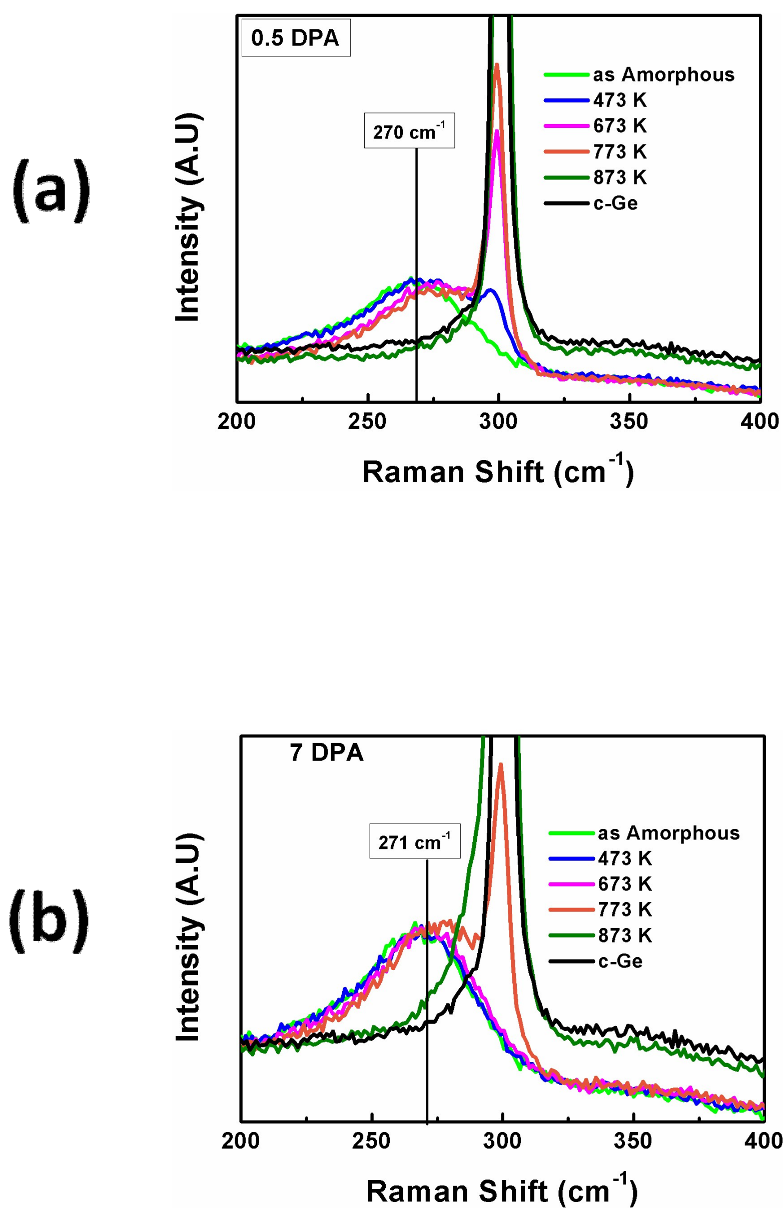

RSC Advances Accepted Manuscript

Fig. 4

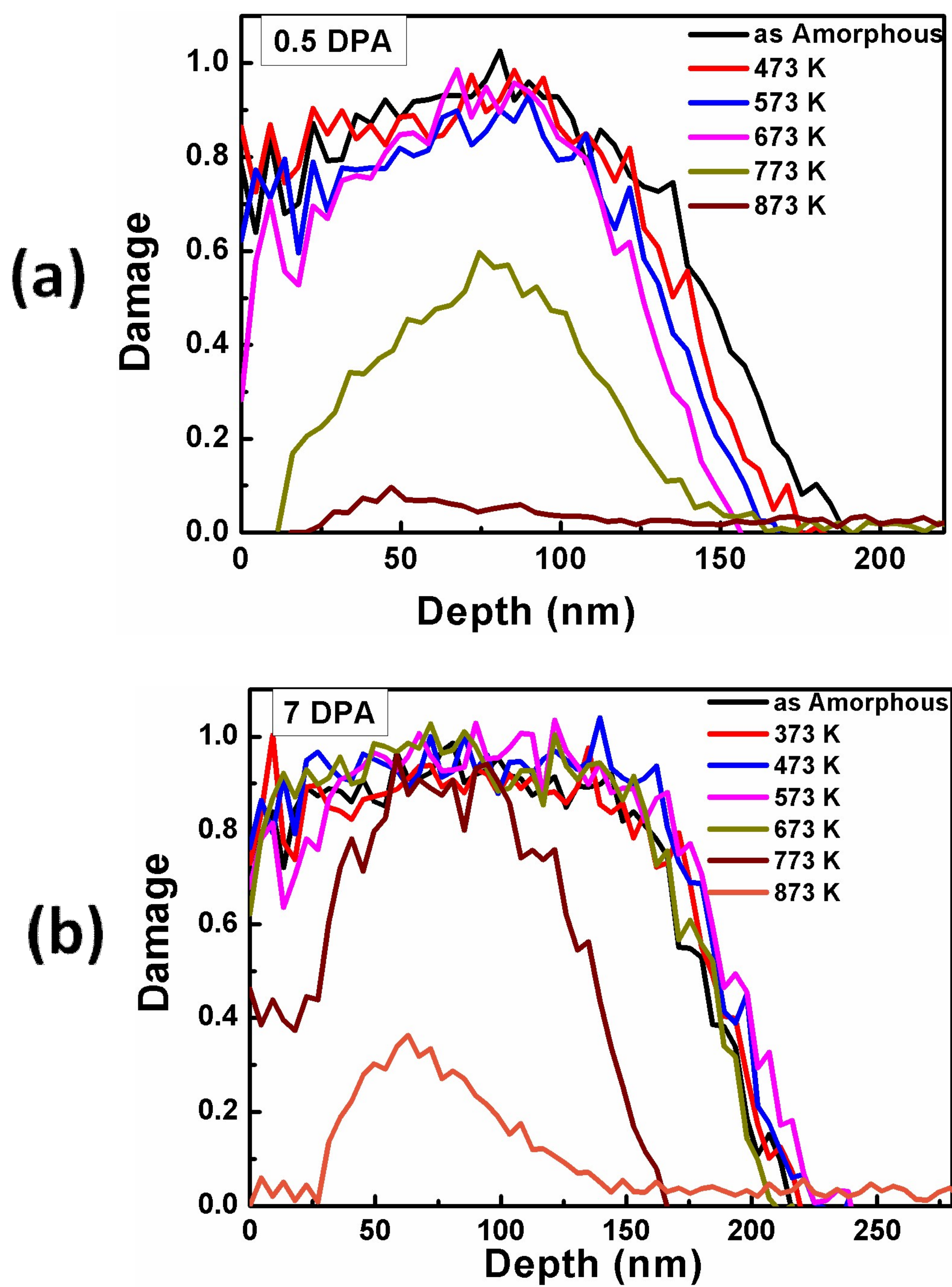

RSC Advances Accepted Manuscript

Fig. 5

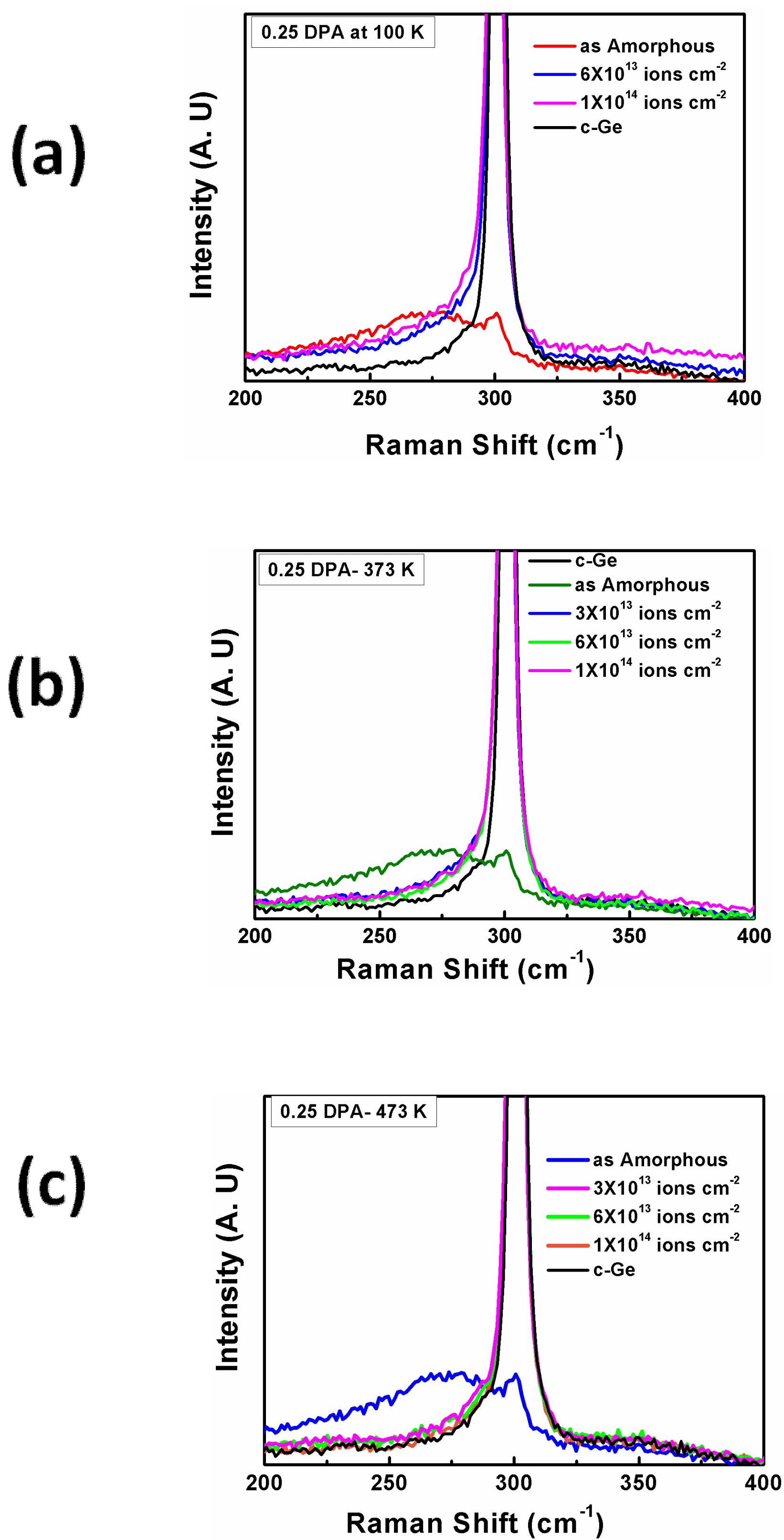

RSC Advances Accepted Manuscript

Fig. 6

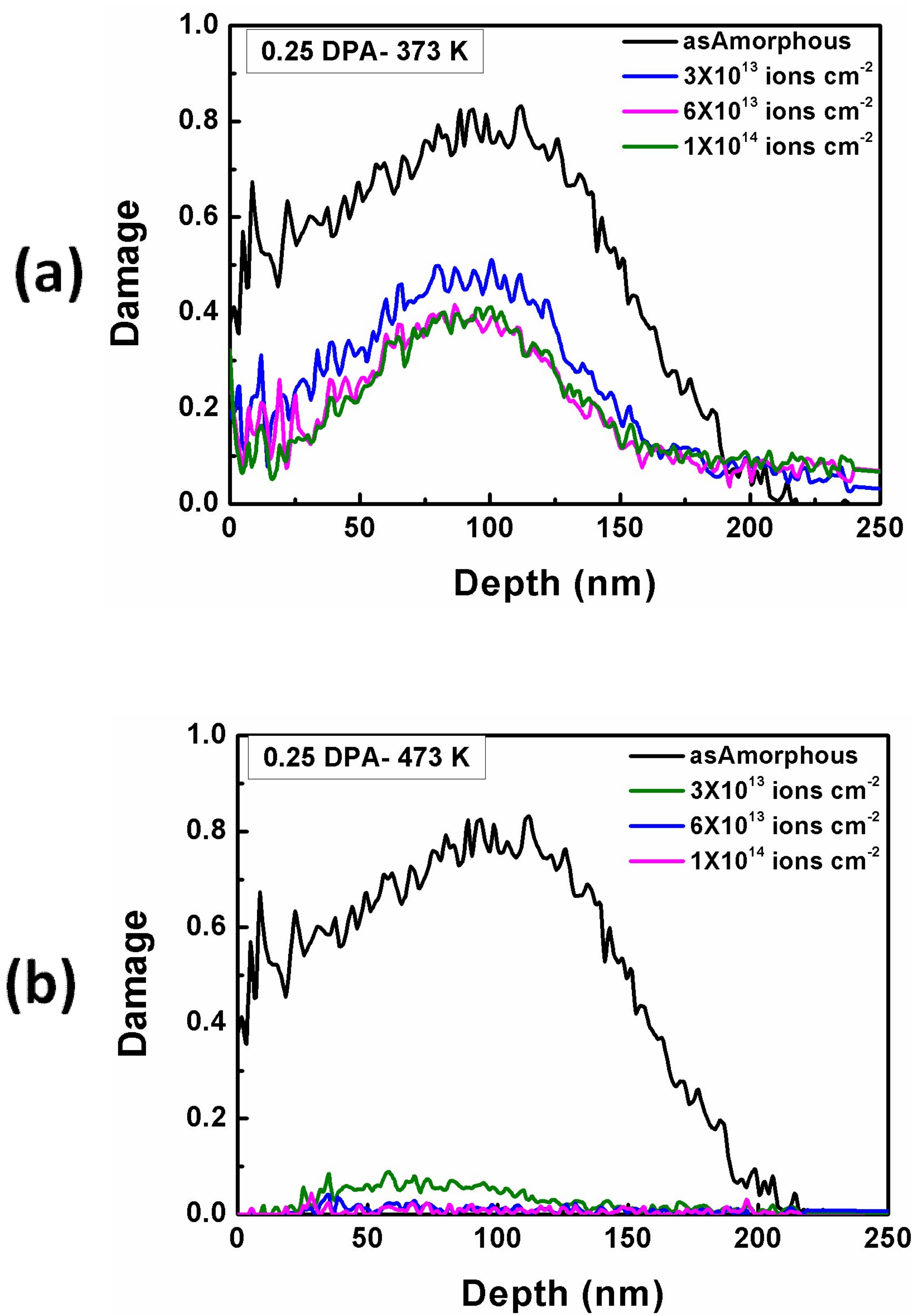

RSC Advances Accepted Manuscript

Fig. 7

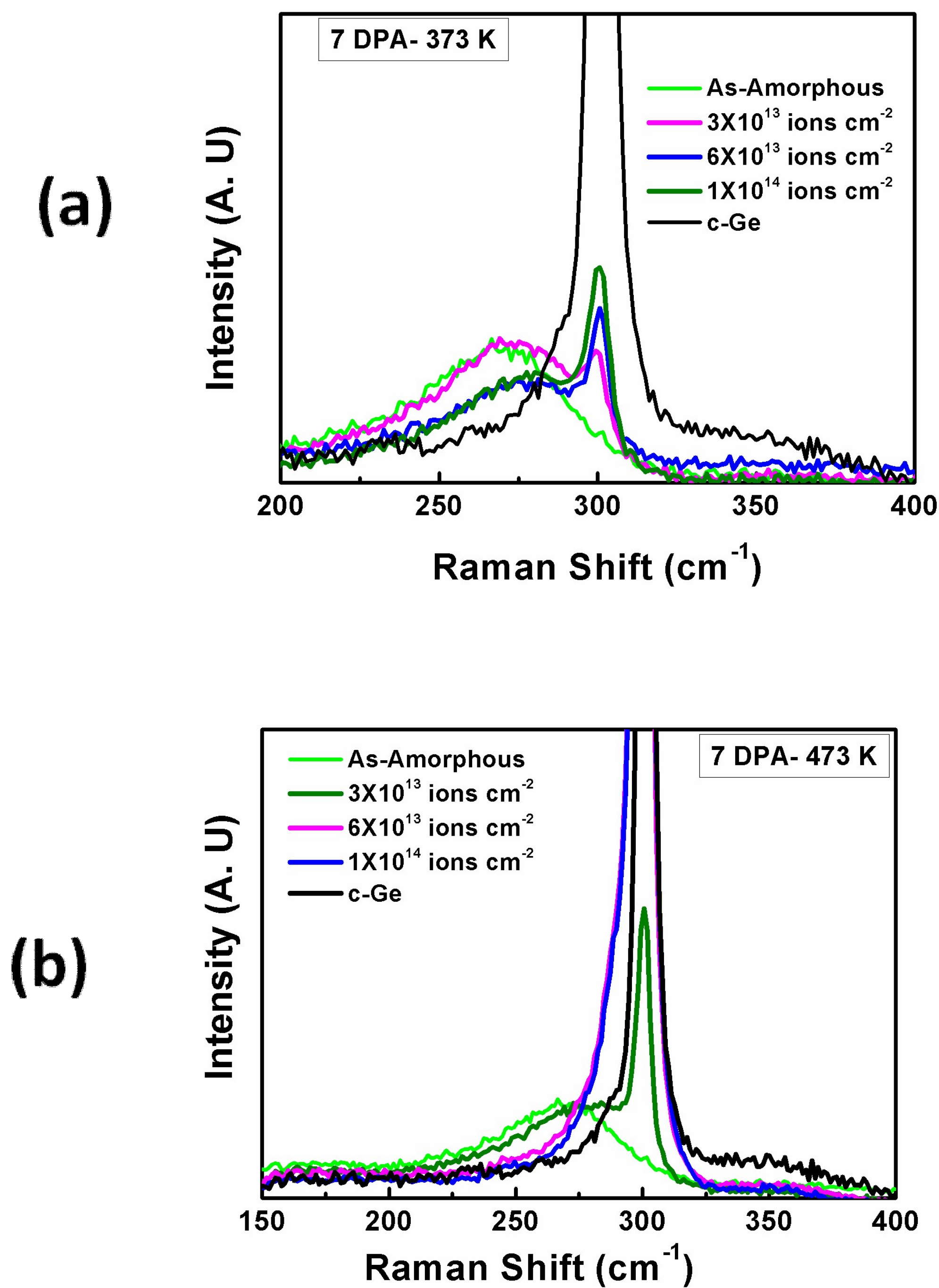

RSC Advances Accepted Manuscript

Fig. 8

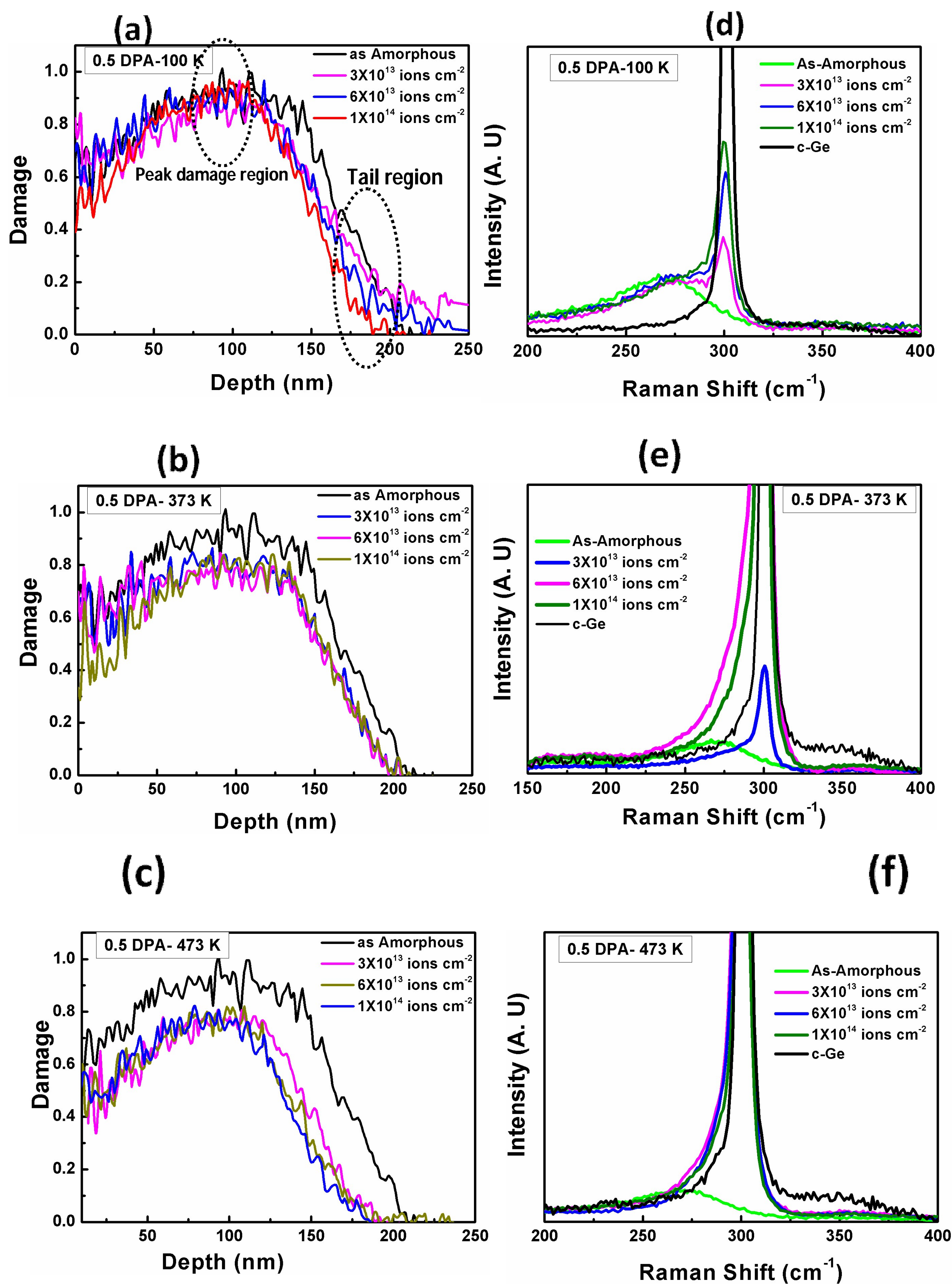

RSC Advances Accepted Manuscript

Fig. 9

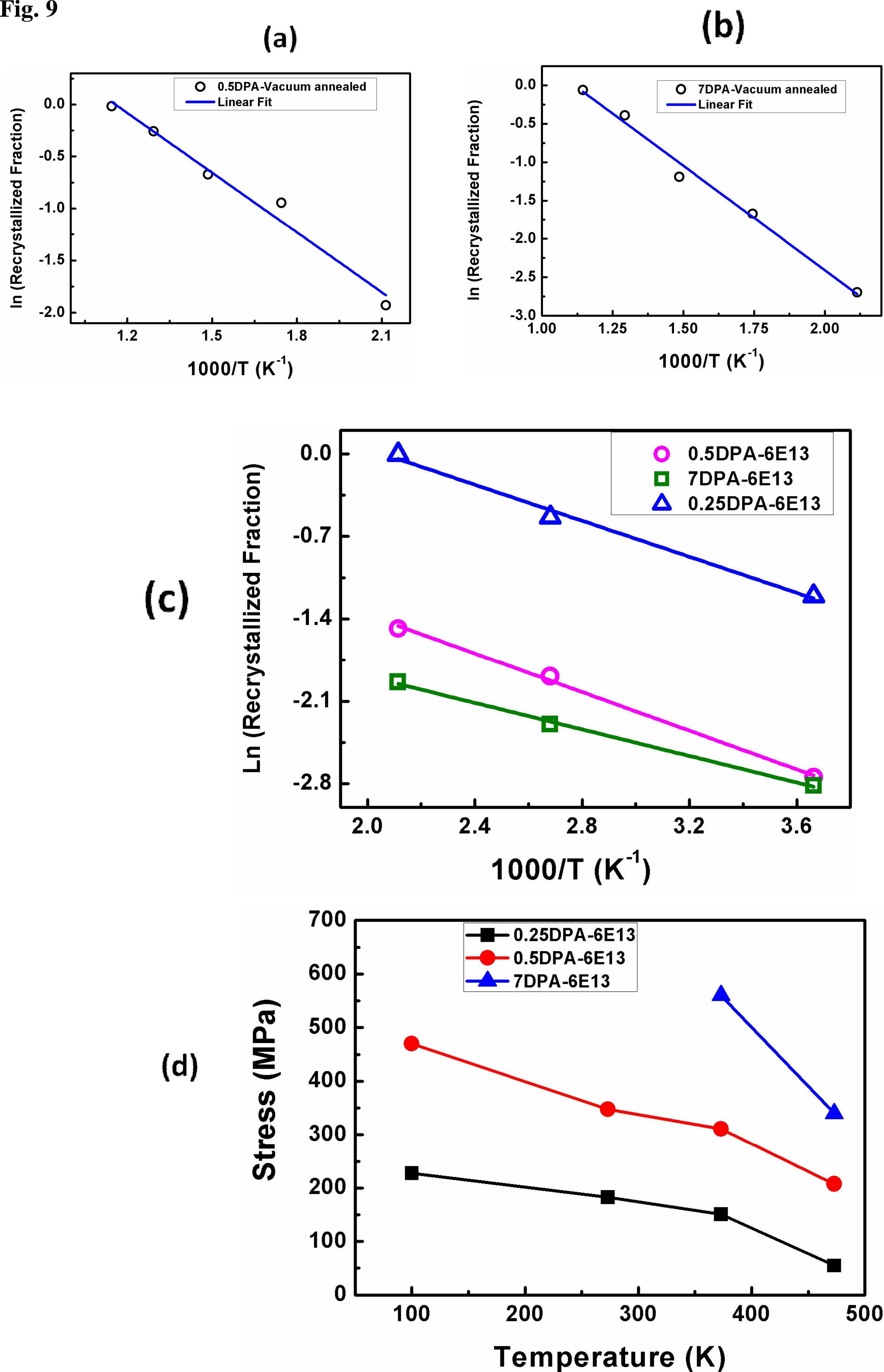

RSC Advances Accepted Manuscript

Fig. 10

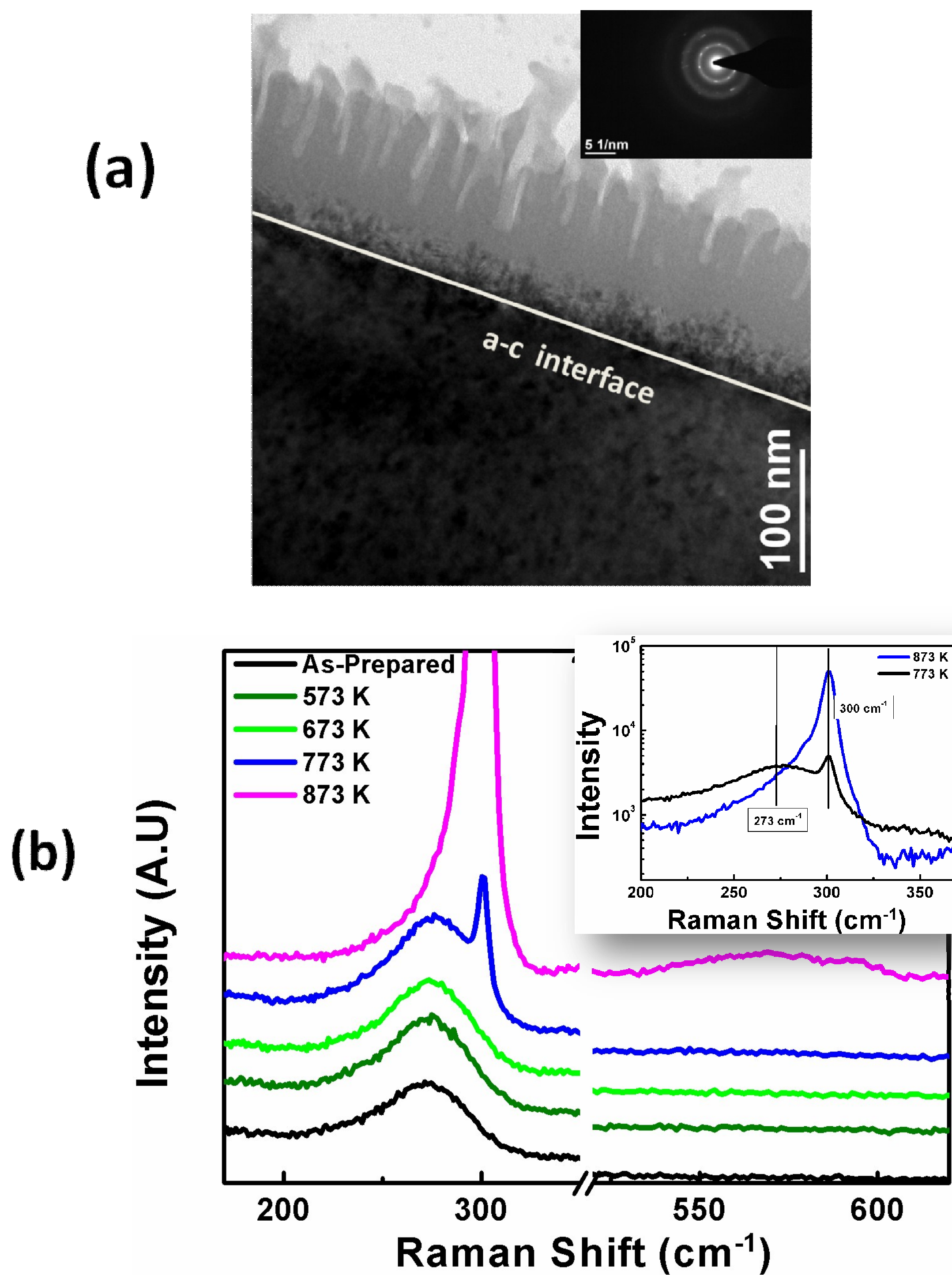

RSC Advances Accepted Manuscript

Fig. 11

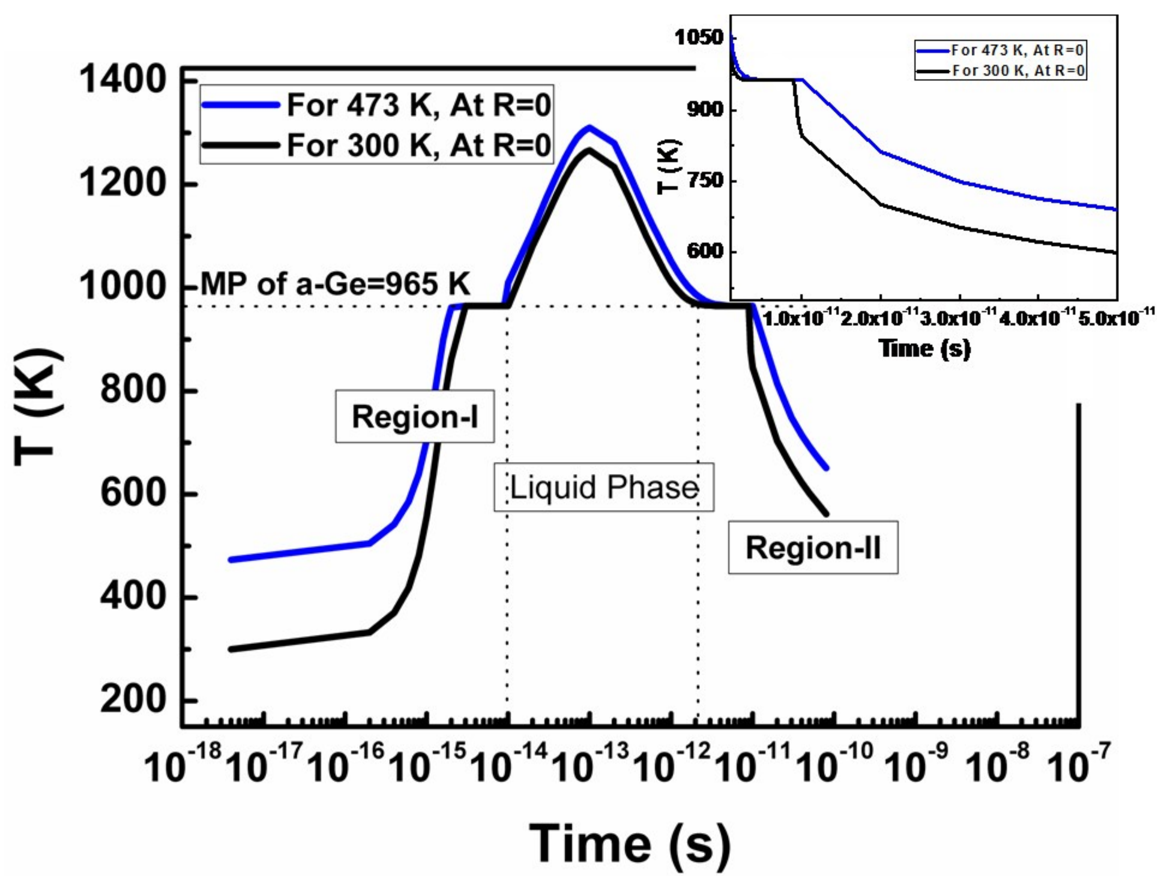

RSC Advances Accepted Manuscript

References

1. C. Claeys and E. Simoen, *Germanium-based technologies: from materials to devices.* (Access Online via Elsevier, 2011).
2. E. Simoen, J. Mitard, G. Hellings, G. Eneman, B. De Jaeger, L. Witters, B. Vincent, R. Loo, A. Delabie, S. Sioncke, M. Caymax and C. Claeys, Materials Science in Semiconductor Processing **15** (6), 588-600 (2012).
3. Y. G. Yoon, T. K. Kim, I.-C. Hwang, H.-S. Lee, B.-W. Hwang, J.-M. Moon, Y.-J. Seo, S. W. Lee, M.-H. Jo and S.-H. Lee, ACS Applied Materials & Interfaces **6** (5), 3150-3155 (2014).
4. L.-H. Zeng, M.-Z. Wang, H. Hu, B. Nie, Y.-Q. Yu, C.-Y. Wu, L. Wang, J.-G. Hu, C. Xie, F.-X. Liang and L.-B. Luo, ACS Applied Materials & Interfaces **5** (19), 9362-9366 (2013).
5. C. Yan, N. Singh, H. Cai, C. L. Gan and P. S. Lee, ACS Applied Materials & Interfaces **2** (7), 1794-1797 (2010).
6. F.-F. Ren, K.-W. Ang, J. Ye, M. Yu, G.-Q. Lo and D.-L. Kwong, Nano letters **11** (3), 1289-1293 (2011).
7. S. Assefa, F. Xia and Y. A. Vlasov, Nature **464** (7285), 80-84 (2010).
8. R. Jones, S. Thomas, S. Bharatan, R. Thoma, C. Jasper, T. Zirkle, N. Edwards, R. Liu, X. Wang and Q. Xie, presented at the IEDm: international electron devices meeting, 2002 (unpublished).
9. M. K. Hudait, M. Clavel, Y. Zhu, P. S. Goley, S. Kundu, D. Maurya and S. Priya, ACS Applied Materials & Interfaces **7** (9), 5471-5479 (2015).
10. T. Kennedy, E. Mullane, H. Geaney, M. Osiak, C. O'Dwyer and K. M. Ryan, Nano letters **14** (2), 716-723 (2014).
11. X. Li, Z. Yang, Y. Fu, L. Qiao, D. Li, H. Yue and D. He, ACS Nano **9** (2), 1858-1867 (2015).
12. S.-K. Kang, G. Park, K. Kim, S.-W. Hwang, H. Cheng, J. Shin, S. Chung, M. Kim, L. Yin, J. C. Lee, K.-M. Lee and J. A. Rogers, ACS Applied Materials & Interfaces **7** (17), 9297-9305 (2015).
13. R. A. Kelly, J. D. Holmes and N. Petkov, Nanoscale **6** (21), 12890-12897 (2014).
14. W. Jiang, H. Wang, I. Kim, I. T. Bae, G. Li, P. Nachimuthu, Z. Zhu, Y. Zhang and W. J. Weber, Phys. Rev. B **80** (16), 161301 (2009).
15. J. F. Gibbons, Proceedings of the IEEE **60** (9), 1062-1096 (1972).
16. J. Nakata, J Appl Phys **79** (2), 682-698 (1996).
17. L. Pelaz, L. A. Marqués and J. Barbolla, J Appl Phys **96** (11), 5947-5976 (2004).
18. P. K. Sahoo, T. Som, D. Kanjilal and V. N. Kulkarni, Nucl. Instr. Meth. Phys. Res. B **240** (1–2), 239-244 (2005).
19. D. Sigurd, G. Fladda, L. Eriksson and K. Björkqvist, Radiation Effects **3** (2), 145-147 (1970).
20. K. Gärtner, J. Jöhrens, T. Steinbach, C. S. Schnohr, M. C. Ridgway and W. Wesch, Phys. Rev. B **83** (22), 224106 (2011).
21. G. Impellizzeri, E. Napolitani, S. Boninelli, G. Fisicaro, M. Cuscuna, R. Milazzo, A. La Magna, G. Fortunato, F. Priolo and V. Privitera, J Appl Phys **113** (11), 113505-113507 (2013).
22. G. S. Armatas and M. G. Kanatzidis, Nano letters **10** (9), 3330-3336 (2010).
23. T. Steinbach, J. Wernecke, P. Kluth, M. C. Ridgway and W. Wesch, Phys. Rev. B **84** (10), 104108 (2011).
24. S. Decoster and A. Vantomme, J Phys D Appl Phys **42** (16), 165404 (2009).
25. P. N. Okholin, V. I. Glotov, A. N. Nazarov, V. O. Yuchymchuk, V. P. Kladko, S. B. Kryvyi, P. M. Lytvyn, S. I. Tiagulskyi, V. S. Lysenko, M. Shayesteh and R. Duffy, Materials Science in Semiconductor Processing.
26. B. L. Darby, B. R. Yates, N. G. Rudawski, K. S. Jones and A. Kontos, Nucl. Instr. Meth. Phys. Res. B **269** (1), 20-22 (2011).
27. C. Wündisch, M. Posselt, B. Schmidt, V. Heera, T. Schumann, A. Mücklich, R. Grötzschel, W. Skorupa, T. Clarysse, E. Simoen and H. Hortenbach, Appl. Phys. Lett. **95** (25), 252107 (2009).
28. J. Bourgoin and J. Corbett, Radiation Effects **36** (3-4), 157-188 (1978).

RSC Advances Accepted Manuscript

29. S. Hooda, B. Satpati, S. Ojha, T. Kumar, D. Kanjilal and D. Kabiraj, Materials Research Express **2** (4), 045903 (2015).
30. T. Som, J. Ghatak, O. P. Sinha, R. Sivakumar and D. Kanjilal, J Appl Phys **103** (12), - (2008).
31. M. Toulemonde, C. Dufour and E. Paumier, Phys. Rev. B **46** (22), 14362-14369 (1992).
32. J. F. Ziegler, M. D. Ziegler and J. P. Biersack, Nucl. Instr. Meth. Phys. Res. B **268** (11–12), 1818-1823 (2010).
33. K. Gärtner, Nucl. Instr. Meth. Phys. Res. B **132** (1), 147-158 (1997).
34. A. Benyagoub and A. Audren, J Appl Phys **106** (8), - (2009).
35. V. Paillard, P. Puech, M. A. Laguna, P. Temple-Boyer, B. Caussat, J. P. Couderc and B. de Mauduit, Appl. Phys. Lett. **73** (12), 1718-1720 (1998).
36. M. C. Ridgway, T. Bierschenk, R. Giulian, B. Afra, M. D. Rodriguez, L. L. Araujo, A. P. Byrne, N. Kirby, O. H. Pakarinen, F. Djurabekova, K. Nordlund, M. Schleberger, O. Osmani, N. Medvedev, B. Rethfeld and P. Kluth, Physical Review Letters **110** (24), 245502 (2013).
37. S. A. Khan, S. K. Srivastava and D. K. Avasthi, J Phys D Appl Phys **45** (37), 375304 (2012).
38. V. Hugouvieux, E. Farhi, M. R. Johnson, F. Juranyi, P. Bourges and W. Kob, Phys. Rev. B **75** (10), 104208 (2007).
39. M. Werner, H. Mehrer and H. D. Hochheimer, Phys. Rev. B **32** (6), 3930-3937 (1985).
40. H. Haesslein, R. Sielemann and C. Zistl, Physical Review Letters **80** (12), 2626-2629 (1998).
41. A. Chroneos and H. Bracht, Applied Physics Reviews **1** (1), 011301 (2014).

RSC Advances Accepted Manuscript

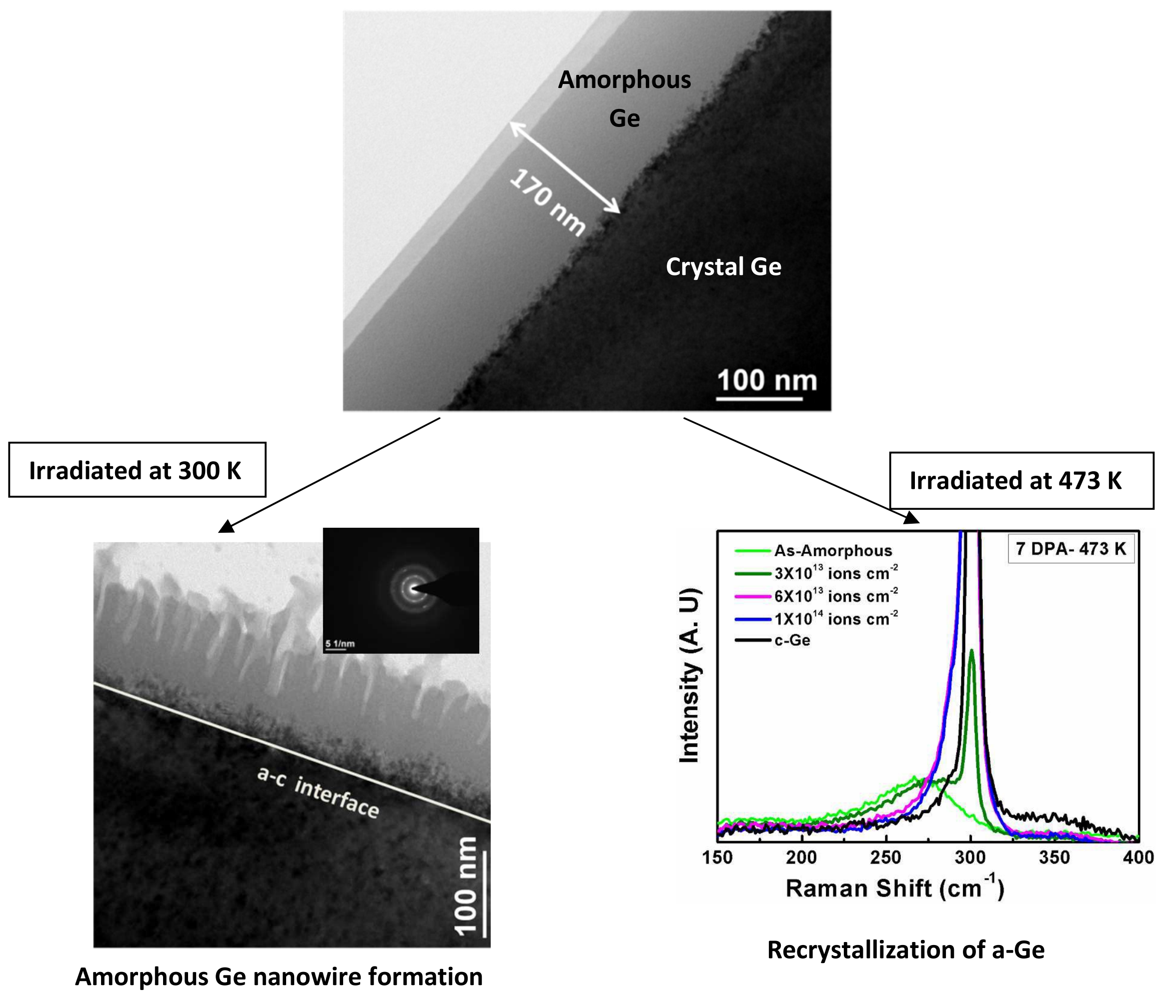

RSC Advances Accepted Manuscript